

# Three types of nonlinear resonances

Arianna Marchionne and Peter Ditlevsen  
*Niels Bohr Institute, University of Copenhagen, Denmark*

Sebastian Wiecezorek  
*Department of Applied Mathematics, University College Cork, Ireland*  
 (Dated: February 15, 2022)

We analyse different types of nonlinear resonances in a weakly damped Duffing oscillator using bifurcation theory techniques. In addition to (i) odd subharmonic resonances found on the primary branch of symmetric periodic solutions with the forcing frequency and (ii) even subharmonic resonances due to symmetry-broken periodic solutions that bifurcate off the primary branch and also oscillate at the forcing frequency, we uncover (iii) novel resonance type due to isolas of periodic solutions that are not connected to the primary branch. These occur between odd and even resonances, oscillate at a fraction of the forcing frequency, and give rise to a complicated resonance ‘curve’ with disconnected elements and high degree of multistability.

We use bifurcation continuation to compute resonance tongues in the plane of the forcing frequency vs. the forcing amplitude for different but fixed values of the damping rate. In this way, we demonstrate that identified here isolated resonances explain the intriguing structure of “patchy tongues” observed for weak damping and link it to a seemingly unrelated phenomenon of “bifurcation superstructure” described for moderate damping.

## INTRODUCTION

The response of non-linear oscillators to external periodic forcing is a surprisingly complex phenomenon. It has been investigated in a whole range of natural systems ranging from biology [1, 2] to glacial cycles [3, 4]. Also, various physical systems, such as lasers [5], electric circuits [6] and mechanical oscillators [7] have been studied through the last century. A widely studied model system of a *damped and forced nonlinear oscillator* is the Duffing oscillator, which is an anharmonic oscillator that can be realised as a mass on a spring with a non-linear restoring force [7–10]:

$$\frac{d^2x}{dt^2} + \gamma \frac{dx}{dt} + \omega_0^2 x + \beta x^3 = A \cos(\omega t). \quad (1.1)$$

Here,  $\beta$  is the strength of the non-linearity,  $\gamma$  is the damping rate,  $A$  is the forcing strength,  $\omega$  is the external forcing frequency, and  $\omega_0$  is the natural frequency for small amplitude oscillations in the undamped and unforced case ( $\gamma = A = 0$ ). By suitably normalising the time  $t$  and position  $x$ , and rescaling  $\gamma, \omega$  and  $A$ , we can set  $\omega_0 = \beta = 1$  without loss of generality and work with just three input parameters. We shall use the term “natural frequency” to refer to the frequency of the undamped and unforced oscillator. This frequency depends on the amplitude of the oscillation  $x_{max}$ . By mechanical energy conservation, the natural frequency can be calculated from the period of oscillation;  $T(x_{max}) = 2 \int_0^{x_{max}} dx/\dot{x}$ , and  $\dot{x}^2/2 = U(x_{max}) - U(x)$ , where the potential  $U(x)$  is obtained from  $-U'(x) = -x - x^3$  [11]. In spite of being one of the simplest nonlinear oscillators, the Duffing oscillator (1.1) exhibits surprisingly rich dynamical behaviour owing to its amplitude-dependent natural frequency. More precisely, as the forcing parameters  $A$  and

$\omega$  are varied, the response can show symmetry-breaking pitchfork bifurcations, period-doubling bifurcations, multistability (multiple attractors for the same parameter settings) and even chaotic oscillations; see [9, 12–14] for an overview.

Whereas recent research has focused on nonlinear oscillators with irregular external signals, there are aspects of classical periodic forcing that have not been fully explored. In this paper, we relate the physical concept of subharmonic resonances and mathematical concept of bifurcations to uncover a novel resonance type. We obtain our main results for an intermediate damping strength  $\gamma = 0.01$ , and use bifurcation continuation techniques [15] to calculate the structure of resonance tongues in the plane of the forcing frequency  $\omega$  and amplitude  $A$ . Furthermore, we describe the difference between resonance and synchronisation [16], and show that the novel resonance is unusual in the sense that it has some of the characteristics of synchronised oscillations. Our results explain the “patchy” tongues observed in recent numerical simulations [13] and link them to previous results on instabilities and chaos due to “bifurcation superstructure” in Eq. (1.1) [12].

In order to define synchronisation, we consider a generalisation of the damped Duffing oscillator (1.1) to the self-sustained Duffing-Van der Pol oscillator:

$$\frac{d^2x}{dt^2} + \gamma(x) \frac{dx}{dt} + x + x^3 = A \cos(\omega t), \quad (1.2)$$

where the damping rate  $\gamma$  can depend on  $x$  and change sign with  $x$ , thus also act as a source of energy into the oscillator when its amplitude becomes small.

### Bifurcation superstructure: Odd and even resonances

Due to the nonlinear term  $x^3$ , which gives rise to amplitude dependent natural frequency, Eq (1.1) exhibits many more resonances in addition to the main harmonic resonance near  $\omega = 1$ . For sufficiently small  $A$  and  $\gamma$ , these resonances occur near  $\omega = 1/k$ . They were first examined in detail by Parlitz and Lauterborn [12] (PL85), who refer to a resonance as odd (even) when  $k$  is odd (even). When  $A$  is increased, the resonances shift away from  $\omega = 1/k$  due to the forcing-induced change in the oscillation amplitude and the resulting shift in the corresponding natural frequency. (PL85) focus on moderate damping rate ( $\gamma = 0.2$ ) and high forcing strength ( $0 < A < 50$ ), and perform numerical bifurcation analysis which reveals self-similar set of bifurcations, referred to as “bifurcation superstructure”, with regions of chaos in the  $(\omega, A)$  parameter plane. They associate the “bifurcation superstructure” with the alternating odd and even resonances.

### Patchy tongues

Paar and Pavin [13] (PP98) discuss coexisting attractors in Eq. (1.1) with weak damping ( $\gamma = 0.001$ ) and moderate forcing strength ( $0 < A < 5$ ) using numerical simulations. This parameter range is devoid of bifurcations giving rise to chaotic oscillations. Instead, (PP98) demonstrate a high degree of multistability between periodic solutions and show an intriguing pattern of patchy tongues in the  $(\omega, A)$  parameter plane; see Fig. 1 which was obtained in the same way as [13, Fig.1] but for  $\gamma = 0.01$ . The colours in Fig. 1 refer to different integer ratios of the period of periodic responses and the period  $2\pi/\omega$  of the forcing. This pattern cannot be explained in terms of even and odd resonances identified in (PL85), and is referred to by (PP98) as “intermingled Arnold tongues”.

In the following analysis we show that the backbone of the intriguing pattern of intermingled tongues from (PP98) is formed by resonance tongues associated with the novel resonance type and not by Arnold tongues. Furthermore, we continue the largest resonance tongue of the novel type from  $\gamma = 0.01$  to  $\gamma = 0.2$ , and link it directly to an element of the “bifurcation superstructure” from (PL85).

## RESONANCE VS. SYNCHRONISATION

In order to illustrate the main differences between the phenomenon of resonance and the phenomenon of synchronisation, we compare in Fig. 2 the structure of the

solutions to the underdamped and forced Duffing oscillator (1.1) with  $\gamma = 0.01$  in panels (a) and (c), and the self-sustained and forced Duffing-Van der Pol oscillator (1.2) with  $\gamma(x) = (1-x^2)\gamma$  in panels (b) and (d). Following are definitions and the listing of the characteristic properties for the two phenomena.

### Resonance

A *resonance* phenomenon is defined for a conservative oscillator ( $\gamma(x) = 0$ ) or a *dissipative oscillator* [ $\gamma(x) > 0$  for some  $x$ ] as a noticeable increase in the amplitude of oscillations near certain forcing frequencies. This is best illustrated by fixing  $A$  and plotting the *resonance curve*: the amplitude of periodic solutions  $x_{max}$  as a function of the forcing frequency  $\omega$ . Classical resonance in damped oscillators has the following properties:

- (r1) In a linear oscillator (i.e. without the  $x^3$  term in Eq. (1.1)), there is only one resonance near the natural frequency. In a nonlinear oscillator, depending on the type of the nonlinearity, there can be additional *subharmonic resonances* when the forcing frequency approaches a fraction or a multiple of the natural frequency [17].
- (r2) Typically, the frequency of the resonant response is the same as the forcing frequency. The frequency of a non-resonant response is also the same as the forcing frequency. (Note: this situation may change for large  $A$  [12].)
- (r3) As defined above, resonance is, in general, a quantitative phenomenon. However, in damped oscillators with amplitude-dependent frequency, resonance may involve bistability and qualitative changes in the solutions namely saddle-node bifurcations of periodic solutions.

For example, Fig. 2(a) shows the resonance curve for the Duffing oscillator (1.1) with  $A = 0.05$  near the main resonance. The resonance curve ‘leans over’ so that there is a range of frequencies with two stable periodic solutions, one of which has a much larger amplitude and corresponds to a resonant response; the two solutions also have different phases. Which of these two solutions the system settles to depends on initial conditions. This bistable range is bounded by two saddle-node bifurcations *SN* of periodic solutions [18], marked with red diamonds in Fig. 2(a). By varying the amplitude and the frequency of the forcing, we have:

- (r4) In the  $(\omega, A)$  parameter plane, the corresponding codimension-one saddle-node bifurcation curves form *resonance tongues*. A resonance tongue has a tip for  $A$  small but nonzero and  $\omega$  near the natural

frequency or near a fraction/multiple of the natural frequency. Moreover, the tip corresponds to a codimension-two cusp bifurcation  $C$  [18], where the two branches of the saddle-node bifurcation curve meet in a tangency [Fig. 2(c)]. Subharmonic resonance tongues appear for larger  $A$  than the harmonic resonance tongue [12].

Note that for large enough  $A$ , resonance tongues may shift in frequency, have additional cusp points and may interact with other bifurcations via special codimension-two bifurcation points. On the other hand, for values of  $A$  below the cusp point  $C$ , the resonance curve does not show any bistability and closely resembles the resonance curve of a damped harmonic oscillator.

### Synchronisation

The phenomenon of  $m:n$  synchronisation, where  $m, n \in \mathbb{N}$ , is defined for a dissipative but *self-sustained oscillator* [e.g.  $\gamma(x) = (1 - x^2)\gamma$  in Eq. (1.2)] as a stable and fixed-in-time relationship between the phases of the forcing  $\phi(t) = \omega t$  and of the oscillator  $\varphi(t)$ :

$$0 < |m\phi(t) - n\varphi(t)| \leq 2\pi \Rightarrow \frac{\omega}{\Omega} = \frac{n}{m},$$

where  $\Omega$  is the frequency of the (forced) oscillator. Classical synchronisation to periodic forcing has the following properties:

- (s1) A nonlinear oscillator can synchronise to periodic external forcing at various forcing frequencies provided that  $m\omega/n$  is sufficiently close to the natural frequency.
- (s2) The frequency of the (periodic) synchronised response is  $\Omega = m\omega/n$ , which by (s1) is close to the natural frequency. However, an unsynchronised response is quasiperiodic, meaning that it has components at the natural frequency, the forcing frequency, and linear combinations of both frequencies.

Fig. 2(b) shows a range of forcing frequencies where the oscillator (1.2) synchronises in the ratio 1:1 to periodic external forcing. The solid curve is a branch of stable periodic solutions corresponding to the synchronised response, while the dashed curve is a branch of unstable periodic solutions. The two branches meet and disappear in a saddle-node bifurcation of periodic solutions at both ends of the synchronisation range [red diamonds in Fig. 2(c)]. Outside the synchronisation range, the incommensurate ratio of the oscillator frequency and the forcing frequency leads to stable quasiperiodic solutions, which appear as disconnected dots in Fig. 2(b). Although resonance and synchronisation involve the same bifurcation type, there are important differences between these two nonlinear phenomena:

- (s3) As defined above, synchronisation is a qualitative phenomenon because synchronisation-desynchronisation transitions correspond to saddle-node bifurcations  $SN$  of periodic solutions [Fig. 2(b)]. However, in contrast to the resonance phenomenon, there is normally just one stable solution at each value of  $\omega$ , meaning that there is no bistability of periodic solutions for small  $A$ . (Note: This may change for large  $A$  where one expects complicated dynamics due to break-up of invariant tori [19, 20] and potentially more than one stable solution.)
- (s4) In the  $(\omega, A)$  parameter plane, the corresponding saddle-node bifurcation curves form  $m:n$  synchronisation tongues or *Arnold tongues* [21, 22]; see Fig. 2(d) for an example of a 1:1 synchronisation tongue in the Duffing-Van der Pol oscillator (1.2). A  $m:n$  synchronisation tongue has a tip at  $A = 0$  and  $\omega = n\omega_0/m$ , where  $\omega_0$  is the frequency of the unforced oscillations. In contrast to the resonance tongue, this tip does not correspond to a cusp bifurcation.

The synchronisation phenomenon is captured in the  $(\omega, A)$  parameter plane by an infinite but countable number of Arnold tongues. Unlike resonance tongues, Arnold tongues originate at  $A = 0$  and  $\omega = n\omega_0/m$ , where  $m, n \in \mathbb{N}$ . As  $A$  is increased, the tongues widen and may shift in frequency but they do not overlap until some critical value of  $A_c > 0$ . Above  $A_c$ , overlapping tongues indicate break-up of invariant tori through various mechanisms including homoclinic tangencies between stable and unstable manifolds of saddle-type periodic solutions like the one indicated with a dashed curve in Fig. 2(b). What is more, for  $A$  large enough, Arnold tongues may shift in frequency and develop cusp points, and will typically interact with other bifurcations at special codimension-two bifurcation points [19, 20]. The model example of Arnold tongues is the circle map [21, 23].

The remainder of this paper focuses on the detailed structure of resonances in the Duffing oscillator.

### COMPLICATED RESONANCE CURVE: THREE RESONANCE TYPES

To explain the high degree of multistability and the intermingled structure of patchy tongues observed in numerical simulations, we investigate the resonance structure in Eq.(1.1). Besides the harmonic resonance depicted in Fig.2(a), there are subharmonic resonances in accordance with property (r1). The resonance curve in Fig. 3 for  $A = 3$  shows that subharmonic resonances: occur for  $\omega < 1$ , become distinct only for larger  $A$  than the one used in Fig.2 (a) and, as  $A$  is increased, the

first to appear are odd subharmonic resonances. Using the notation adopted from (PL85) we denote by  $R_k$  the (subharmonic) resonances occurring when  $\omega = (\text{natural frequency})/k$ .

### Conventional Resonances

The periodic solutions represented in the resonance curve are found using the numerical continuation techniques AUTO [15], which also allows detection of unstable periodic solutions. In Fig. 4 we zoom in on the subharmonic resonances from Fig. 3. Here it is seen that parts of the resonance curve are ‘punctuated’ by intervals of unstable periodic solutions. There are two types of punctuation. Firstly, in the odd resonances ( $k > 1$  and odd), the stable and unstable solutions merge in saddle-node bifurcations  $SN$  (diamonds in Fig. 4). Secondly, the unstable solutions found between the odd resonances are bounded by pairs of pitchfork bifurcations  $P$  (squares in Fig. 4). These bifurcations give rise to pairs of stable symmetry-broken periodic solutions, shown in red in Fig. 5, which appear as mirror imaged orbits  $x \leftrightarrow -x$  in the  $(x, \dot{x})$  plane [insets in Fig. 5] [9, 12]. These solutions correspond to even subharmonic resonances ( $k > 1$  and even) and become distinct for  $A$  larger than the odd subharmonic resonances. What is more, they themselves undergo saddle-node bifurcations giving rise to regions of multistability of symmetry-broken periodic solutions.

Both bifurcation types, that is  $SN$  and  $P$ , indicate qualitative changes in the solutions associated with (subharmonic) resonances in accordance with property (r3). Interestingly, the odd and even resonances alone cannot explain the patchy tongue structure from Fig. 1. This means that there must be additional periodic solutions which are not connected to the primary branch [black curve in Fig. 5].

### Isolated Resonances

Figure 6 shows a one-dimensional bifurcation diagram obtained by direct time integration starting with the same initial condition  $(x(0), \dot{x}(0)) = (0, 0)$  for each value of  $\omega$ . A comparison with Fig. 5, obtained using continuation techniques, reveals stable periodic solutions that belong to stable branches of the resonance curve from Fig. 5, as well as additional stable periodic solutions that are not present in Fig. 5. These additional solutions are symmetric period-3 oscillations shown in Fig. 7. What is more, numerical continuation initiated from numerical data for these additional solutions reveals that they form “isolas” disconnected from the primary branch of periodic solutions [green branches are disconnected from the black and red branches in Fig. 8].

We have now from Fig. 4 through Fig. 5 to Fig. 8 identified three different resonance types:

- (i) *Odd resonances* which occur on the branch of primary (symmetric) periodic solutions that oscillate at the forcing frequency (black),
- (ii) *Even resonances* due to symmetry-broken periodic solutions which bifurcate off the primary branch and also oscillate at the forcing frequency (red),
- (iii) *Isolated resonances* due to isolas of periodic solutions with greatly increased amplitude of oscillations (green). This novel resonance is unusual in the sense that it has certain properties akin to synchronised oscillations. Firstly, unlike  $R_k$  resonances, the frequency of oscillation is a fraction of the forcing frequency. Secondly, the periodic solutions involved are bounded by saddle-node bifurcations in a way which is reminiscent of Fig. 2(b) rather than Fig. 2(a). As a consequence, cusp points at low  $A$  are not expected in the corresponding resonance tongues.

Altogether, the three resonance types contribute to a complicated resonance curve in Fig. 8, consisting of various subharmonic resonances and disconnected components, which give rise to many regions of multistability.

### RESONANCE TONGUES

The three resonance types which were identified in the complicated resonance curve from Fig. 8 can be defined in terms of saddle-node (diamonds) and pitchfork (squares) bifurcation points. In the two-dimensional  $(\omega, A)$  parameter plane, these bifurcation points can be continued with AUTO to obtain the corresponding bifurcation curves which are referred to as resonance tongues [property (r4)]. Fig. 9 shows the resonance tongues computed for all three types of resonances. These include: (black) saddle-node bifurcations of the primary branch of periodic solutions which correspond to odd subharmonic resonances, (red) pitchfork bifurcations on the primary branch of periodic solutions which correspond to even subharmonic resonances, (blue) saddle-node bifurcations of the symmetry-broken periodic solutions which give rise to multistability of even resonances, and (green) saddle-node bifurcations bounding the isolas which correspond to isolated resonances.

### Explaining the “patchy tongue structure”

The structure of the resonance tongues bears strong resemblance to the “intermingled Arnold tongues” reported by (PP98) (Fig. 1). We can now superimpose the periodic solutions oscillating at various fractions of the forcing frequency from Fig. 1 obtained by direct time integration and the resonance tongues from Fig. 9 obtained by continuation. The resulting Fig. 10 reveals perfect match

between the (green) resonance tongues corresponding to the isolated resonances and (red) regions with stable periodic solutions oscillating at a third of the forcing frequency. Thus, the intriguing patchy tongue structure found in (PP98) and shown in Fig. 1 can be identified with the isolated resonances, which appear to form the backbone of the structure. Furthermore, the patchiness of the tongues is a result of multistability: there are multiple stable periodic solutions of different frequency for the same parameter settings and, as the initial condition is fixed but the parameters  $\omega$  and  $A$  are varied, the system can settle to a different periodic solution.

There are additional isolated resonances with stable periodic solutions oscillating at  $\omega/n$  for  $n = 2, 4, 5, \dots$ , whose resonance tongues match the remaining patchy tongues from Fig. 1. For clarity, these additional isolated resonance tongues are left out in Fig. 10.

### Links to “bifurcation superstructure”

Our analysis of the intermediate damping rate  $\gamma = 0.01$  and moderate forcing strength  $0 < A < 6$  reveals various periodic solutions and their bifurcations. However, we have not found any bifurcations, such as torus bifurcations or period-doubling cascades, that would eventually lead to irregular or chaotic oscillations. Rather, the saddle-node and pitchfork bifurcations give rise to regions of multistability of periodic solutions.

As the damping rate  $\gamma$  is decreased, the patchy tongues become more abundant. This was demonstrated by (PP98) for  $\gamma = 0.001$ . Hence, isolated resonances become even more prominent at low damping, where they appear at even lower  $A$  and give rise to a greater degree of multistability of periodic solutions.

On the other hand, as the damping rate is increased, isolated resonances seem to give way to the “bifurcation superstructure” involving period-doubling cascades, period-3 solutions and chaotic attractors, which were reported for  $\gamma = 0.2$  and  $10 < A < 50$  by (PL85).

An interesting question emerges whether isolated resonances are purely a low-damping phenomenon or whether the period-3 solutions associated with isolated resonances (Fig. 7) are related to the “bifurcation superstructure” from [12]. To address this question we continued the largest isolated resonance tongue from Fig. 9 to higher values of  $\gamma$ . The results of the continuation are shown in Fig. 11. As  $\gamma$  is increased from  $\gamma = 0.01$  [Fig. 11(a)], the isolated resonance tongue moves to higher values of  $A$  and develops another tip [Fig. 11(b-c)]. At  $\gamma = 0.2$  the continuation of the isolated resonance tongue matches exactly an element of the “bifurcation superstructure” denoted with  $R_{9,3}$  in [12, Fig. 6]. Thus, in addition to explaining “patchy tongues”, isolated resonances (i) provide a link between “patchy tongues” the “bifurcation superstructure” and (ii) give new insight into “bifurcation

superstructure” [12] which now appears to be organised by three rather than two different resonance types.

The key difference is that periodic solutions involved in isolated resonances at low  $\gamma$  may cease to be isolated as  $\gamma$  is increased. The bifurcation diagram in Fig. 12(a), obtained using continuation techniques [15] for  $\gamma = 0.2$ ,  $A = 25$  and  $1.15 \leq \omega \leq 1.7$ , shows the primary branch of periodic solutions (black), the symmetry-broken solutions bifurcating off the primary branch (red) via pitchfork bifurcation (square), two potentially isolated components of periodic solutions (green), and symmetry-broken solutions (blue) bifurcating from the left potentially isolated component via pitchfork bifurcation (square). In Fig. 12(b), a numerical bifurcation diagram obtained starting on the stable branch of each (green) potentially isolated component is superimposed on the continuation results from panel (a). The right-hand side component turns out to be isolated. However, the larger left-hand side component is connected to other solutions. Starting at the stable periodic solution of this component and decreasing  $\omega$ , the solution loses stability via symmetry-breaking pitchfork bifurcation, then the symmetry-broken solution undergoes period-doubling cascade to chaos, followed by an inverse period-doubling cascade to period-one solution (red) which, in turn, connects to the primary branch of periodic solutions (black) via pitchfork bifurcation.

### CONCLUSION

We have investigated nonlinear resonances in terms of bifurcations of periodic solutions using the example of a periodically forced Duffing oscillator. We have identified novel isolated resonances in addition to already known odd and even subharmonic resonances, and demonstrated a complicated resonance ‘curve’ with isolas (isolated components) of periodic solutions and high degree of multistability. Most importantly, the identified here isolated resonances in conjunction with numerical continuation techniques allowed us to (i) explain the intriguing structure of “patchy tongues” observed in stability diagrams for weak damping and (ii) link those “patchy tongues” to a seemingly unrelated phenomenon of “bifurcation superstructure” found for moderate damping.

Firstly, to avoid confusion between resonance and synchronisation, we have defined each phenomenon in terms of bifurcations, gave a short discussion of the key differences, and described how the two phenomena exhibit themselves in the stability diagrams. In particular, we have distinguished between resonance tongues and synchronisation tongues, which are also known as Arnold tongues, in the parameter plane of the forcing frequency vs. the forcing amplitude. Secondly, we have shown that resonance tongues associated with the isolated resonances form the backbone of the intriguing pattern of

“patchy tongues” at weak damping, which were reported by Paar and Pavin and mistaken for Arnold tongues [13]. Thirdly, we have demonstrated that, as the damping rate increases, these resonances may cease to be isolated and the corresponding resonance tongues evolve into particular elements of the “bifurcation superstructure” reported by Parlitz and Lauterborn for moderate damping [12].

The new insight into nonlinear resonances in the simple Duffing oscillator can be extended to more complicated systems. One example are class-B lasers which exhibit damped oscillations (relaxation oscillation onto the lasing solution) and self-sustained oscillations (the lasing solution itself) at the same time. Stability diagrams for lasers subject to external optical injection [24, Figs. 9-11] show variety of coexisting tongues, which can be interpreted as a combination of a 1:1 synchronisation tongue and different types of nonlinear resonance tongues.

- 
- [1] R. FitzHugh, *Biophysics J* **1**, 445 (1961).
  - [2] J. Nagumo, S. Arimoto, and S. Yoshizawa, *Proceedings of the IRE* **50**, 2061 (1962).
  - [3] M. Crucifix, *Philosophical Transactions of the Royal Society of London A: Mathematical, Physical and Engineering Sciences* **370**, 1140 (2012).
  - [4] B. De Saedeleer, M. Crucifix, and S. Wieczorek, *Climate Dynamics* **40**, 273 (2013).
  - [5] S. Wieczorek, B. Krauskopf, T. Simpson, and D. Lenstra, *Physics Reports* **416**, 1 (2005).
  - [6] B. Van der Pol, *The London, Edinburgh, and Dublin Philosophical Magazine and Journal of Science* **2**, 978 (1926).
  - [7] G. Duffing, *Erzwungene Schwingungen bei veränderlicher Eigenfrequenz (Forced vibration with variable natural frequency)*, Vol. 41/42 (F. Vieweg, Braunschweig, 1918).
  - [8] P. Holmes and D. Rand, *Journal of Sound and Vibration* **44**, 237 (1976).
  - [9] P. Holmes, *Philosophical Transactions of the Royal Society of London A: Mathematical, Physical and Engineering Sciences* **292**, 419 (1979).
  - [10] J. Guckenheimer and P. Holmes, *Nonlinear oscillations, dynamical systems, and bifurcations of vector fields*, Vol. 42 (Springer Science & Business Media, 2013).
  - [11] R. Feynman, R. Leighton, and M. Sands, *The Feynman Lectures on Physics*, 2nd ed., Vol. 1 (Addison-Wesley, Boston, 1963).
  - [12] U. Parlitz and W. Lauterborn, *Physics Letters A* **107**, 351 (1985).
  - [13] V. Paar and N. Pavin, *Phys. Rev. E* **57**, 1544 (1998).
  - [14] I. Kovacic and M. J. Brennan, *Background: On Georg*

*Duffing and the Duffing Equation* (John Wiley & Sons, Ltd, 2011).

- [15] E. Doedel and B. Oldeman, “Auto-07p: Continuation and bifurcation software for ordinary differential equations. concordia university,” (2009).
- [16] A. Pikovsky, M. Rosenblum, and J. Kurths, *Synchronization: a universal concept in nonlinear sciences*, Vol. 12 (Cambridge university press, 2003).
- [17] W. Lauterborn, *The Journal of the Acoustical Society of America* **59**, 283 (1976).
- [18] Y. A. Kuznetsov, *Elements of applied bifurcation theory* (Springer, 1998).
- [19] S. Ostlund, D. Rand, J. Sethna, and E. Siggia, *Physica D: Nonlinear Phenomena* **8**, 303 (1983).
- [20] H. Broer, C. Simó, and J. C. Tatjer, *Nonlinearity* **11**, 667 (1998).
- [21] P. L. Boyland, *Comm. Math. Phys.* **106**, 353 (1986).
- [22] J. Norris, *Nonlinearity* **6**, 1093 (1993).
- [23] E. Ott, *Chaos in dynamical systems* (Cambridge university press, 2002).
- [24] B. Krauskopf and S. Wieczorek, *Physica D: Nonlinear Phenomena* **173**, 97 (2002).

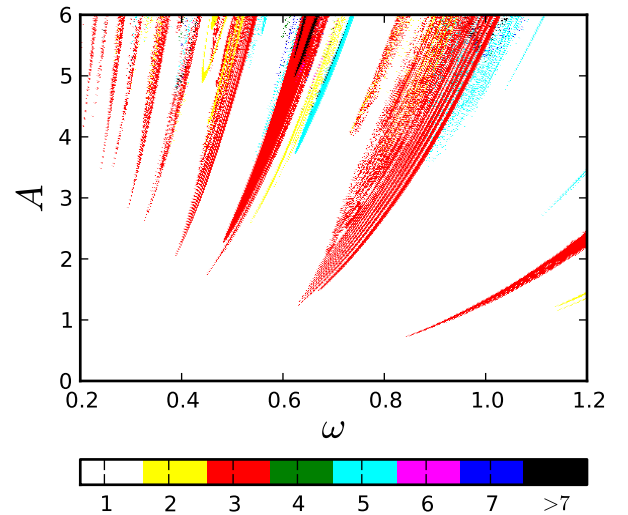


**Figure 1:** Values of parameters  $A$  and  $\omega$  where we find attracting periodic orbits of the Duffing’s system (1.1) of frequency (blank)  $\omega$ , (yellow)  $\omega/2$ , (red)  $\omega/3$ , (green)  $\omega/4$ , (cyan)  $\omega/5$ , (magenta)  $\omega/6$ , (blue)  $\omega/7$ , and (black)  $\omega/n$  for  $n = 8, 9, \dots$ . We used  $\gamma = 0.01$  and initial conditions  $x(0) = \dot{x}(0) = 0$ .

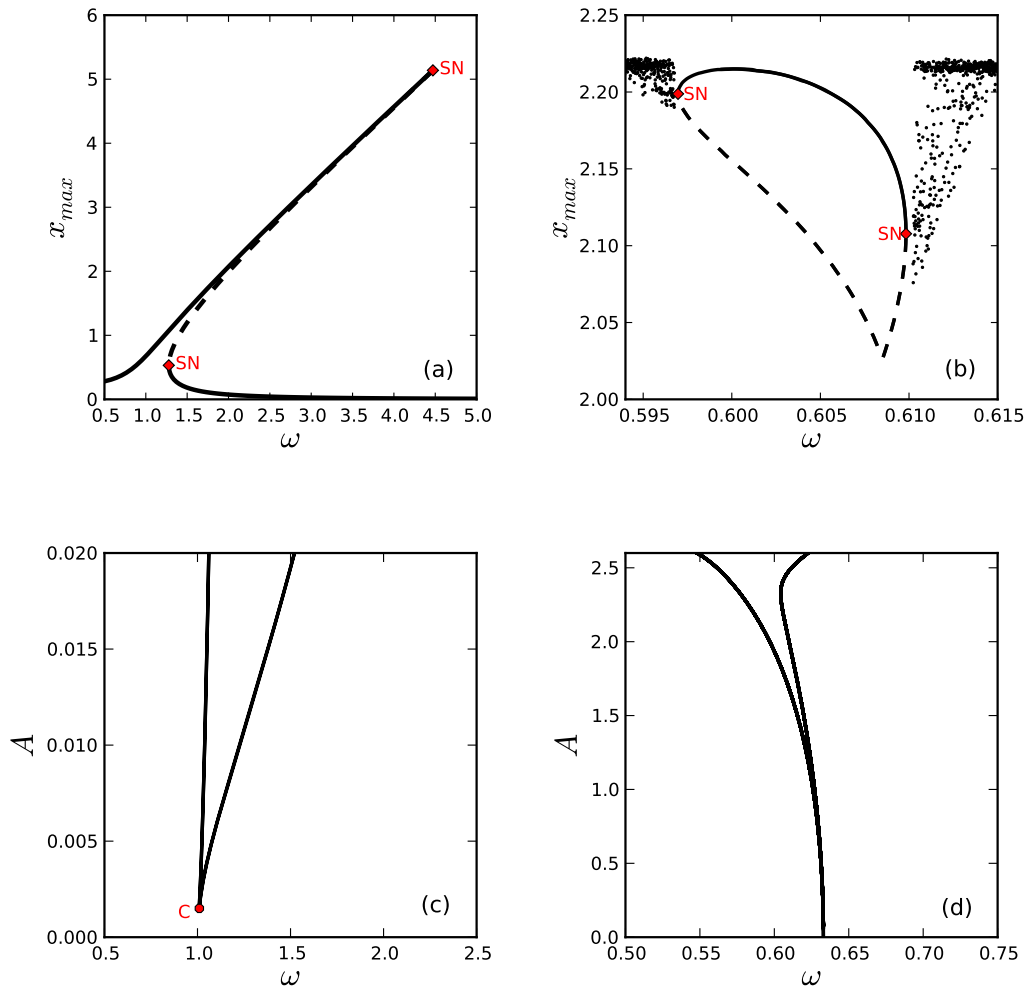


**Figure 2:** (a) Amplitude resonance curve showing the primary resonance of the Duffing's system (1.1). The black solid lines mark the stable solutions, the black dashed lines mark the unstable solutions connecting the two stable ones. Saddle-node bifurcations (SN) are marked by the red diamonds. Fixed parameters and initial condition:  $A = 0.05$ ,  $\beta = 1$ ,  $\gamma = 0.01$ ;  $x(0) = 0$ ,  $\dot{x}(0) = 0$ . (b) Values of the maximum of  $x$  as a function of  $\omega$  showing periodic and quasi-periodic oscillations of the Duffing-Van der Pol system (1.2). Periodic solutions are surrounded by quasi-periodic orbits (black dots). The black solid line marks the stable solutions, the black dashed line marks the unstable solutions. Fixed parameters and initial condition:  $A = 2.0$ ,  $\beta = 1$ ,  $\gamma = 0.01$ ;  $x(0) = \dot{x}(0) = 0$ . (c) Two parameter continuation  $(\omega, A)$  of the saddle-node bifurcations shown in panel (a). The cusp bifurcation C, where the two saddle-node bifurcations merge, is marked by the red circle. Note that the cusp occur for  $A > 0$ . (d) Two parameter continuation  $(\omega, A)$  of the saddle-node bifurcations shown in panel (b).

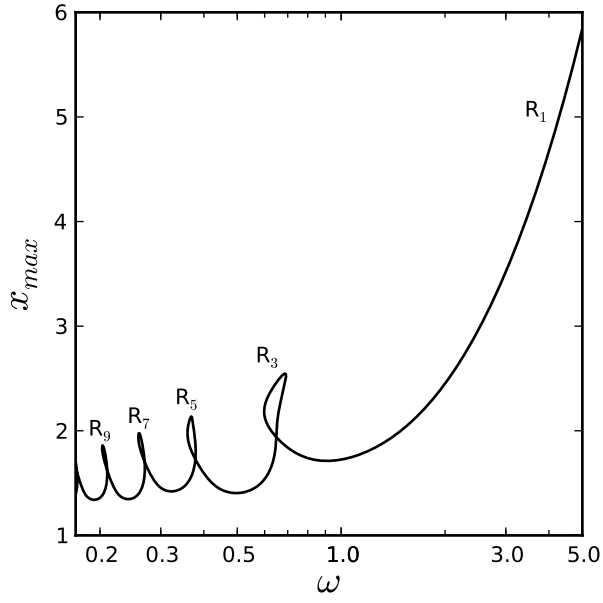


**Figure 3:** Amplitude resonance curve showing the maximum of the coordinate  $x$  of the Duffing equation (1.1) as a function of the forcing frequency  $\omega$ . The curve is obtained with the numerical continuation method AUTO. Fixed parameters:  $A = 3$ ,  $\gamma = 0.01$ .



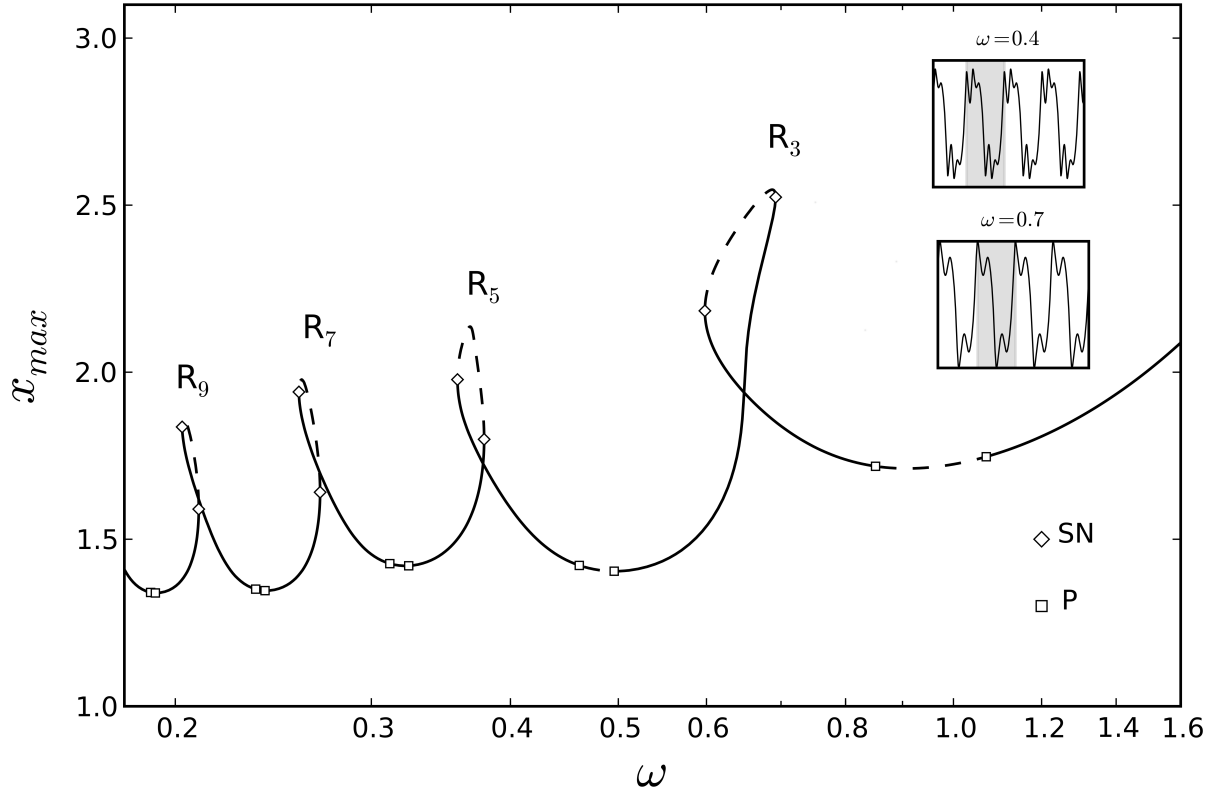


**Figure 4:** Part of the resonance curve in Fig.3 with branches of periodic solutions as a function of the forcing frequency  $\omega$ . On the primary branch of symmetric periodic solutions (black curve), saddle-node bifurcations (diamonds) and pitchfork bifurcations (squares) take place. Stable branches are marked by solid lines, unstable branches by dashed lines. Fixed parameters:  $A = 3$ ,  $\gamma = 0.01$ . The inserts show two solutions in the  $(t, x)$  plane; for  $\omega = 0.4$  the solution is on the  $R_5$  branch, where there are 5 local maxima in one period, marked by the gray band. For  $\omega = 0.7$  the solution is on the  $R_3$  branch, where there are 3 local maxima in one period.

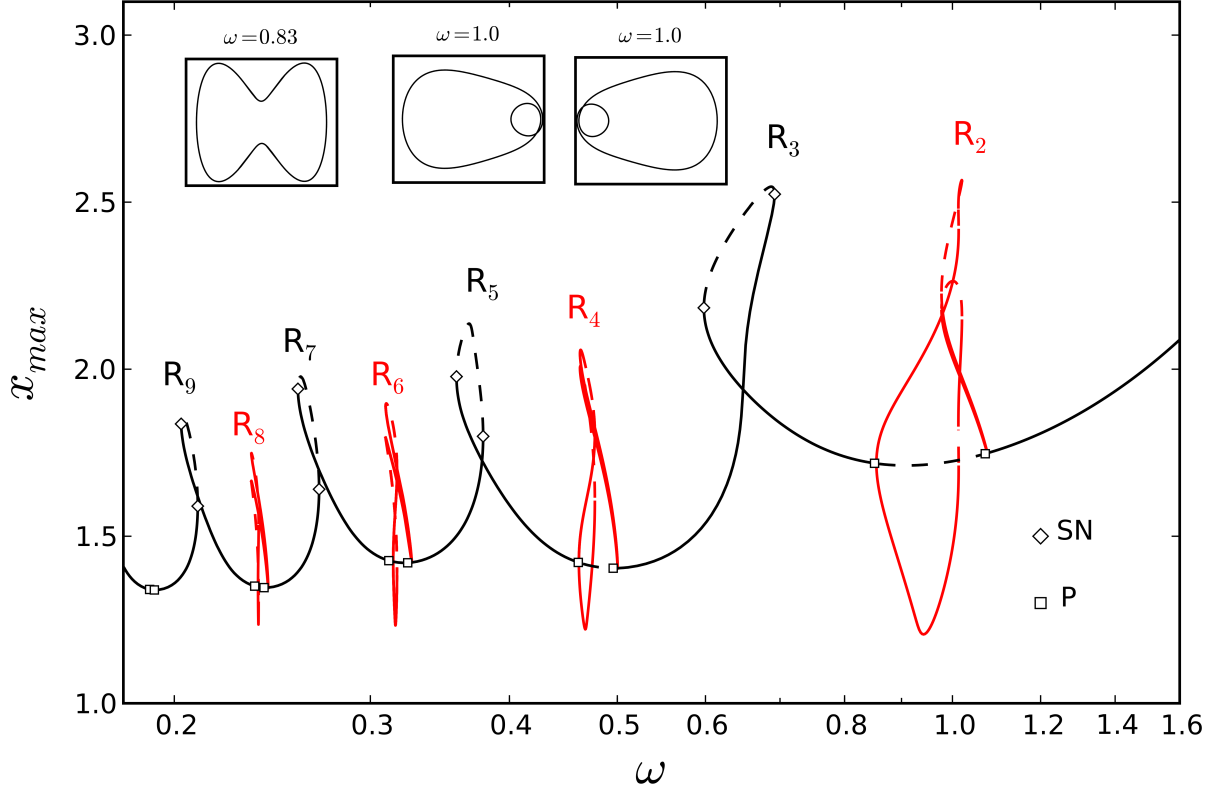


**Figure 5:** Same as Fig.4, now including even resonances: on the primary branch of symmetric periodic solutions (black curve), saddle-node bifurcations (diamonds) and pitchfork bifurcations (squares) take place. At pitchfork bifurcations, pairs of stable symmetry-broken solutions appear (red curves). Stable branches are marked by solid lines, unstable branches by dashed lines. Fixed parameters:  $A = 3$ ,  $\gamma = 0.01$ . Inserts show phase space trajectories  $(x, \dot{x})$  just before a pitchfork bifurcation ( $\omega = 0.83$ ) and a pair of solutions after the  $x \rightarrow -x$  symmetry breaking ( $\omega = 1.0$ ).

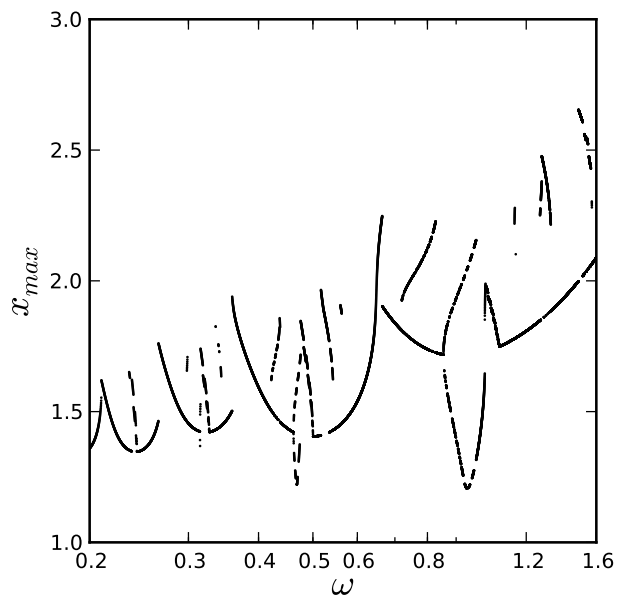


**Figure 6:** 1D numerical bifurcation diagram showing the maximum of  $x$  plotted versus  $\omega$  for  $\gamma = 0.01$ ,  $A = 3$ ,  $x(0) = \dot{x}(0) = 0$ .

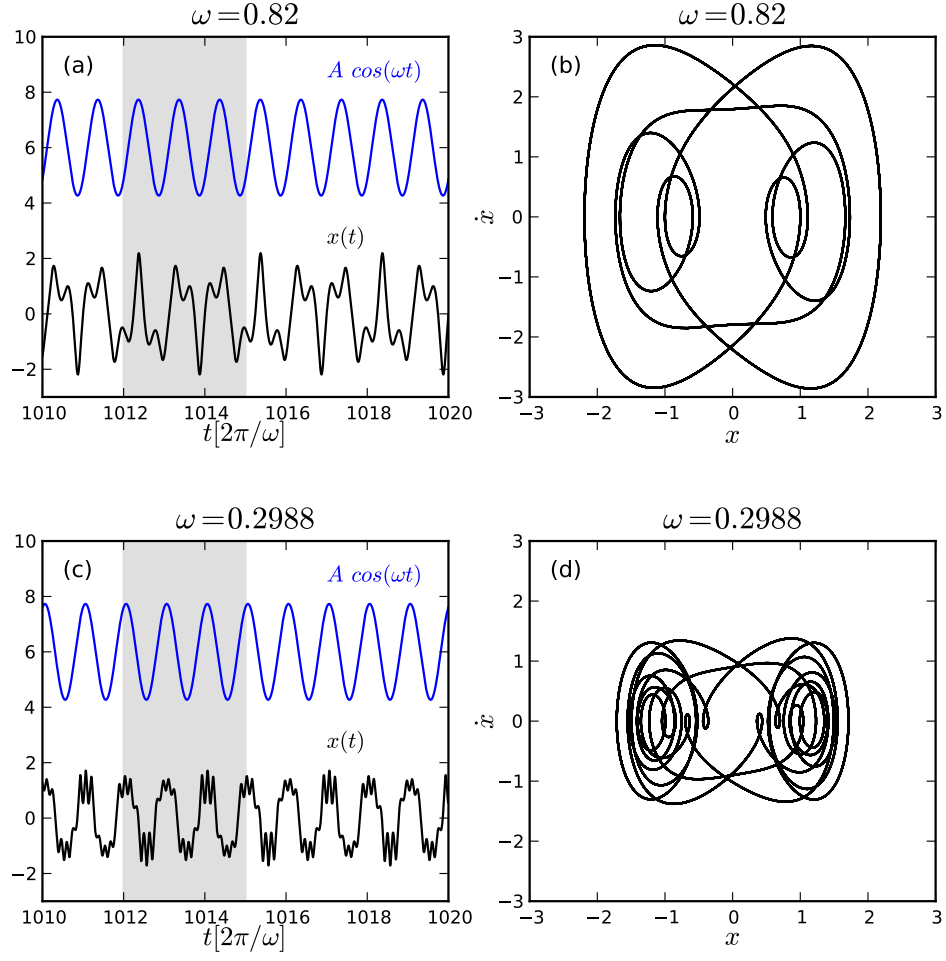


**Figure 7:** Equation (1.1) has been integrated over 1020 periods of the forcing. The additional attracting orbits of the Duffing's system are shown for the last 10 periods of the forcing in the  $(t, x)$  and  $(x, \dot{x})$  planes. The solutions are period-3 orbits indicated by the gray bands. Fixed parameters and initial condition:  $A = 3$ ,  $\gamma = 0.01$ ,  $x(0) = \dot{x}(0) = 0$ . (a) Trajectory in the  $(t, x)$  plane,  $\omega = 0.82$ . (b) Phase space portrait in the two-dimensional  $(x, \dot{x})$  phase space,  $\omega = 0.82$ . (c) Trajectory in the  $(t, x)$  plane,  $\omega = 0.2988$ . (d) Phase space portrait in the two-dimensional  $(x, \dot{x})$  phase space,  $\omega = 0.2988$ .

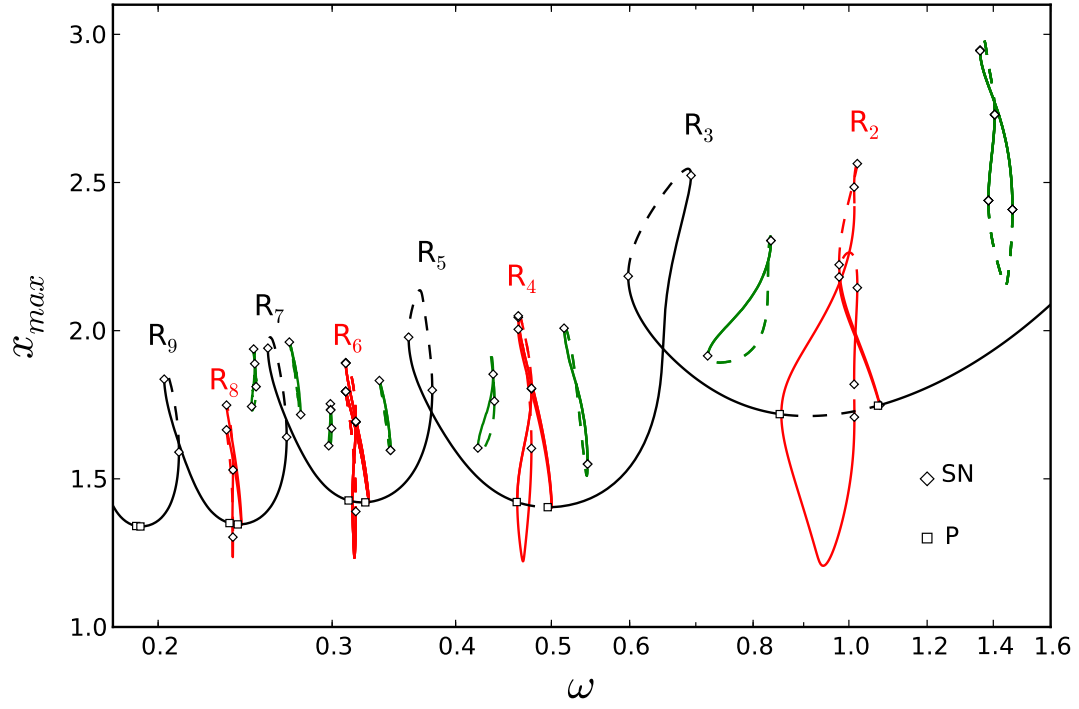


**Figure 8:** Same 1D bifurcation diagram as Figures 4 and 5, but now showing three different types of resonances: Resonances occurring on the symmetric branch of periodic solutions (black curve), resonances occurring on the asymmetric branch of periodic solutions (red curves), isolated resonances (green curves). Stable branches are marked by solid lines, unstable branches by dashed lines. Fixed parameters:  $A = 3$ ,  $\gamma = 0.01$ .

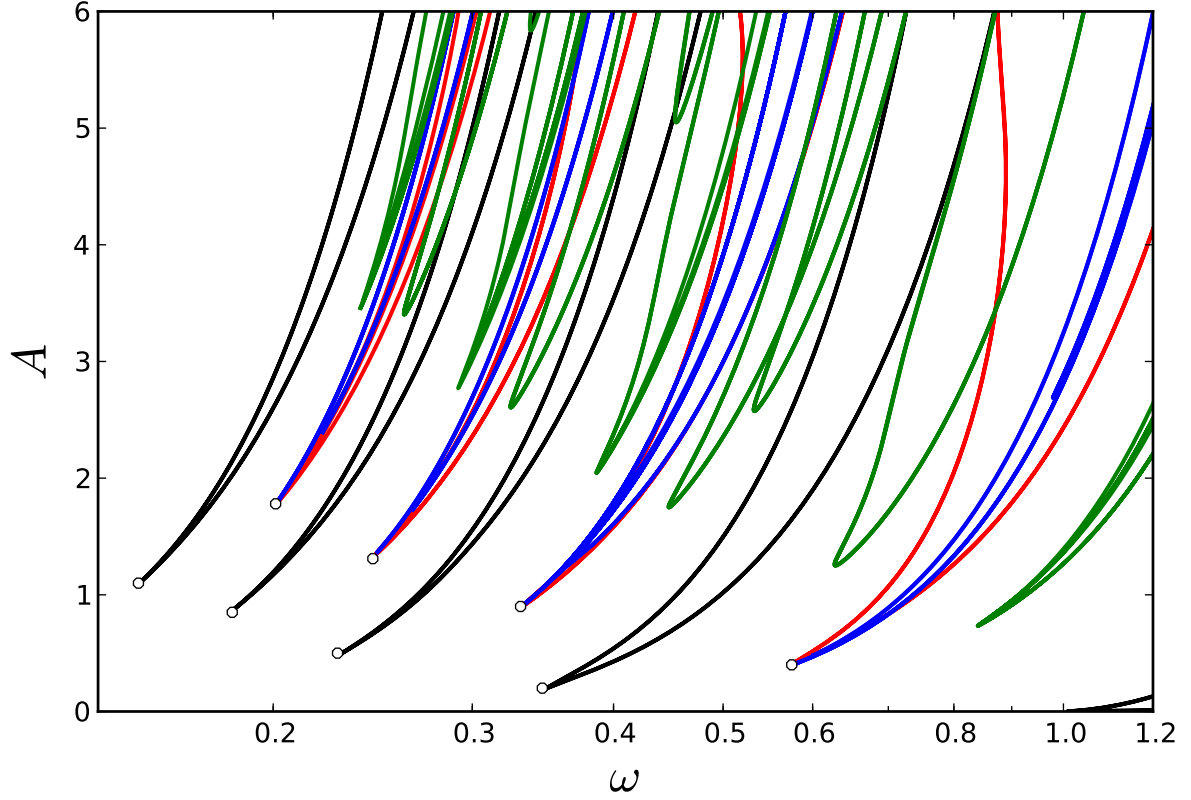


**Figure 9:** Resonance tongues computed for all three types of resonances. These include: (black) saddle-node bifurcations of the primary branch of periodic solutions which correspond to odd subharmonic resonances, (red) pitchfork bifurcations on the primary branch of periodic solutions which correspond to even subharmonic resonances, (blue) saddle-node bifurcations of the symmetry-broken periodic solutions which give rise to multistability of even resonances, and (green) saddle-node bifurcations bounding the isolas which correspond to isolated resonances. Using the notation adopted in (PL85), the resonance tongues computed for the resonance type (i) (*odd resonances*) are denoted by  $R_{1,1}$ ,  $R_{3,1}$ ,  $R_{5,1}$ ,  $R_{7,1}$ ,  $R_{9,1}$ , and the resonance tongues computed for the resonance type (ii) (*even resonances*) are denoted by  $R_{2,1}$ ,  $R_{4,1}$ ,  $R_{6,1}$ ,  $R_{8,1}$ . The first subscript indicates the winding number (here defined as the number of maxima or minima of the periodic solution in one period) and the second subscript is the period in unit of the forcing period  $2\pi/\omega$ . The open circles indicate cusp bifurcations. Fixed parameter:  $\gamma = 0.01$ .

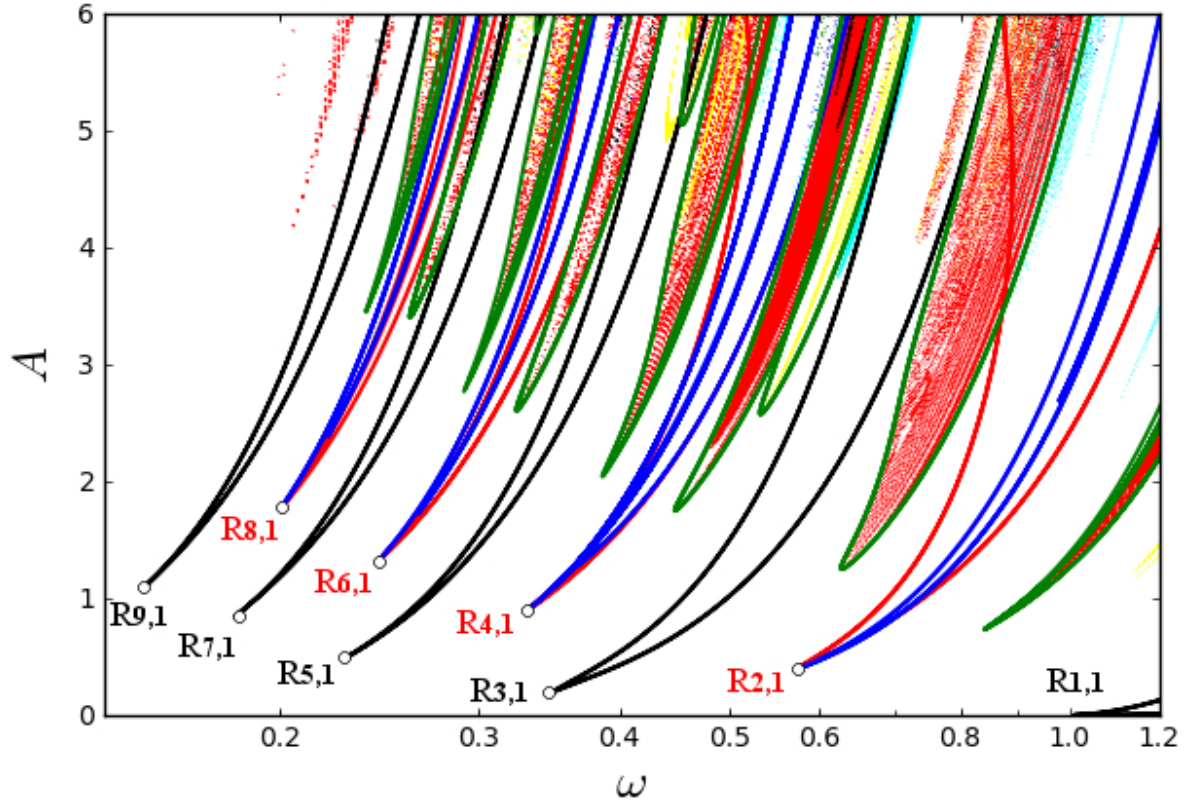


**Figure 10:** Numerical estimates of parameters  $A$  and  $\omega$  leading to periodic attracting trajectories of period  $nT_F$ ,  $n = 1, \dots, 7$  (same as Fig.1) and the bifurcation boundaries of the resonance tongues obtained with the numerical continuation method AUTO are superimposed. The (red) regions with stable period-3 solutions and the (green) resonance tongues corresponding to the isolated resonances match perfectly. The open circles indicate cusp bifurcations.

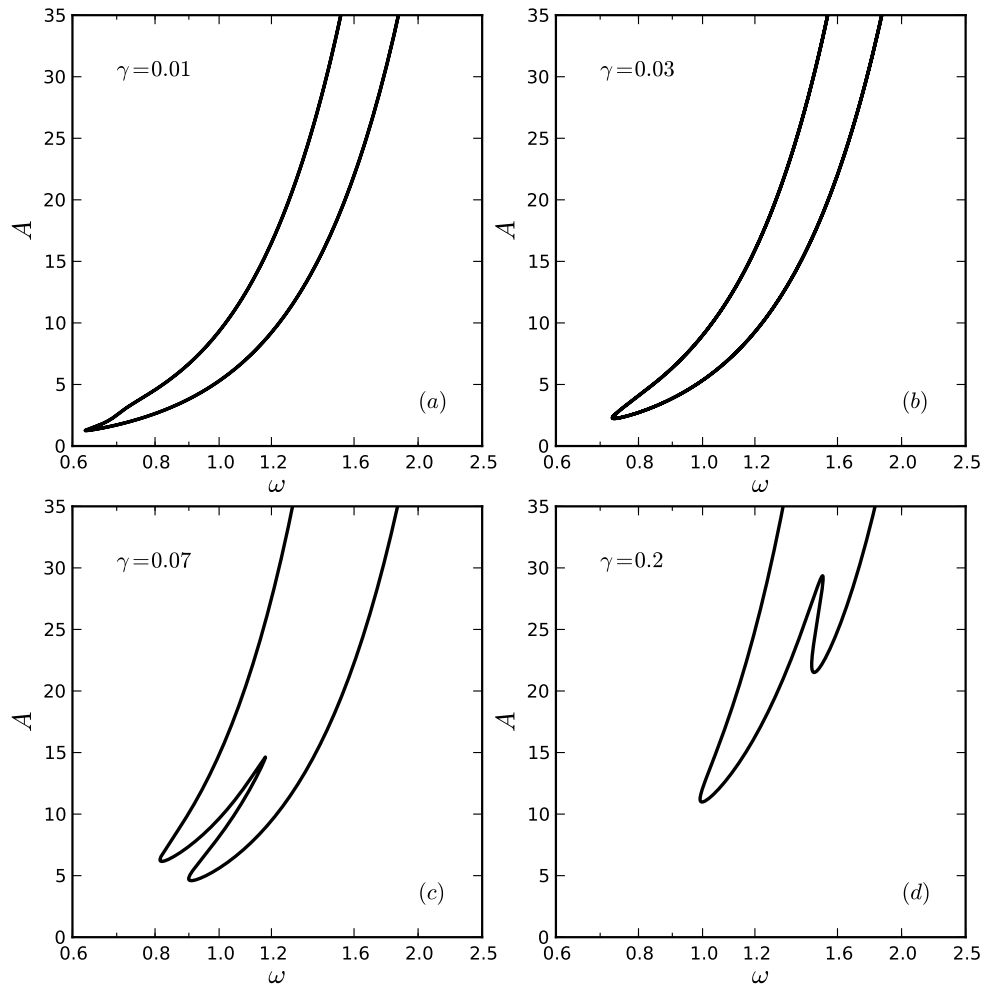


**Figure 11:** Bifurcation curve of the largest isolated resonance for different values of the damping parameter  $\gamma$ .



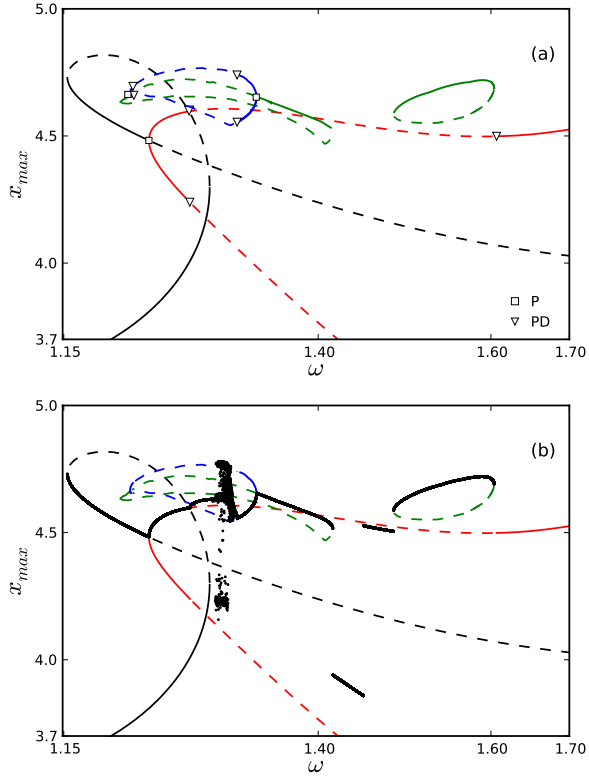


**Figure 12:** (a) AUTO bifurcation diagram in the range  $1.15 < \omega < 1.7$  showing the primary branch of periodic solutions (black), symmetry-broken solutions bifurcating off the primary branch (red), isolas of periodic solutions (green), and symmetry-broken solutions bifurcating from the left isola (blue). (b) A numerical bifurcation diagram is superimposed on the AUTO continuation. The numerical bifurcation diagram consists of four runs: starting at the stable right and left isolas of periodic solutions, the control parameter is increased and decreased.